

HYPERBOLIC SCHWARZ MAPS OF THE AIRY AND THE CONFLUENT HYPERGEOMETRIC DIFFERENTIAL EQUATIONS AND THEIR ASYMPTOTIC BEHAVIORS

TAKESHI SASAKI AND MASAOKI YOSHIDA

ABSTRACT. The Schwarz map of the hypergeometric differential equation is studied first by Schwarz, and later by several authors for various generalizations of the hypergeometric equation. But up to now nothing is studied about the Schwarz map for confluent equations, mainly because such a map would produce just a chaos. Recently we defined the *hyperbolic Schwarz map*, and studied in several cases, including confluent hypergeometric ones, geometric properties of the image surfaces in the hyperbolic 3-space. In this paper, we first study the hypergeometric Schwarz map of the Airy equation, which can be regarded as the doubly confluent hypergeometric equation. The image surface has triangular cuspidal edge curve, and at the three vertices it has three swallowtails. We present some global behaviors by examining the asymptotic behavior of Airy functions at infinity. We next describe the asymptotic behavior of the hyperbolic Schwarz map of the confluent hypergeometric differential equation, which includes the Bessel differential equation; we thus complement the previous study for the confluent hypergeometric equation in [SSY].

CONTENTS

1. Introduction	2
2. Image surface and its singularity	2
2.1. Singularities of flat fronts	2
2.2. Solutions of the equation (A)	3
2.3. Invariance of the hyperbolic Schwarz map	3
3. The Airy functions and the confluent hypergeometric functions	4
3.1. Properties of the Airy functions	4
3.2. Asymptotic behavior of the Airy functions	5
3.3. The confluent hypergeometric functions	6
3.4. Stokes lines of the confluent hypergeometric functions	7
4. Image surface for the Airy differential equation	7
4.1. Image of a fan around the line $\arg x = 0$	7
4.2. Image of a fan around the line $\arg x = \pi/3$	8
4.3. Image of rings around the origin	8
4.4. Change of image of rings	11
5. Asymptotic behavior of the hyperbolic Schwarz map associated with the confluent hypergeometric equation	14
Acknowledgments	15
References	16

Date: January 7, 2008.

2000 Mathematics Subject Classification. 33C05, 53C42.

Key words and phrases. Airy differential equation, hyperbolic Schwarz map, swallowtail singularity.

1. INTRODUCTION

For an equation of the form

$$(E) \quad u'' - q(x)u = 0$$

defined in a domain $X \in \mathbf{P}^1$, where q is a rational function in x , we defined in [SYY1] the hyperbolic Schwarz map

$$\mathcal{S} : x \mapsto H(x) = U(x) {}^t\bar{U}(x) \in \mathbf{H}^3, \quad U = \begin{pmatrix} u_0 & u'_0 \\ u_1 & u'_1 \end{pmatrix},$$

where the hyperbolic 3-space \mathbf{H}^3 is defined to be the space of positive-definite hermitian 2-matrices modulo positive reals, and $\{u_0, u_1\}$ are linearly independent solutions of (E). We identify \mathbf{H}^3 with the 3-ball $\mathbf{B}^3 = \{(y_1, y_2, y_3) \mid y_1^2 + y_2^2 + y_3^2 < 1\}$ by combining the following two maps, where $L_1 = \{(x_0, x_1, x_2, x_3) \mid x_0^2 - x_1^2 - x_2^2 - x_3^2 = 1\}$ is the hypersphere in the Lorenz-Minkowski 4-space:

$$\text{Her}^+(2) \ni \begin{pmatrix} h & \bar{w} \\ w & k \end{pmatrix} \mapsto \frac{1}{2\sqrt{hk - |w|^2}} (h + k, w + \bar{w}, -i(w - \bar{w}), h - k) \in L_1,$$

and

$$L_1 \ni (x_0, x_1, x_2, x_3) \mapsto (y_1, y_2, y_3) = \frac{1}{1 + x_0} (x_1, x_2, x_3) \in \mathbf{B}_3.$$

Through this identification, the image surface is drawn in the ball. The hyperbolic Schwarz map \mathcal{S} is singular along the curve $\{x \in X \mid |q(x)| = 1\}$; its image C will be called the cuspidal edge curve, since at generic points the image has cuspidal edge singularities.

In this paper, we study this map for the differential equation

$$(A) \quad u'' - q(x)u = 0 \quad \text{where} \quad q(x) = x^{k-2}, \quad k = 3, 4, \dots$$

When $k = 3$, this equation is called the Airy differential equation. We see that the image surface S of the x -plane $X = \mathbf{C}$ under \mathcal{S} has cuspidal edge singularities along the k -gon C except at the k cuspidal vertices, where S has swallowtail singularities. To visualize the surface S , we examine the asymptotic behavior of the map \mathcal{S} and we see that the surface S tends to three circles along the Stokes lines and to the particular three points along the open sectors as the point approaches to the irregular singular point at infinity.

In the paper [SSY], we studied the hyperbolic Schwarz map associated with the confluent hypergeometric differential equation

$$(C) \quad u'' - q(x)u = 0 \quad \text{where} \quad q = \frac{x^2 + 2ax + b}{4x^2},$$

where a and b are assumed to be real constants. We remark that the Bessel differential equation corresponds to the case $a = 0$. The asymptotic behavior of this map at infinity is also given.

2. IMAGE SURFACE AND ITS SINGULARITY

2.1. Singularities of flat fronts. It is known that the map \mathcal{S} defines a surface called flat front and its singularities are generically cuspidal edge singularities or swallowtail singularities. Refer to [KRSUY, SYY1].

The following criterion is known:

Lemma 2.1. ([KRSUY]).

- (1) A point $x \in X$ is a singular point of the hyperbolic Schwarz map S if and only if $|q(x)| = 1$,
- (2) a singular point $x \in X$ is a cuspidal edge if and only if $q'(x) \neq 0$ and $(q^3\bar{q}' - q')(x) \neq 0$,

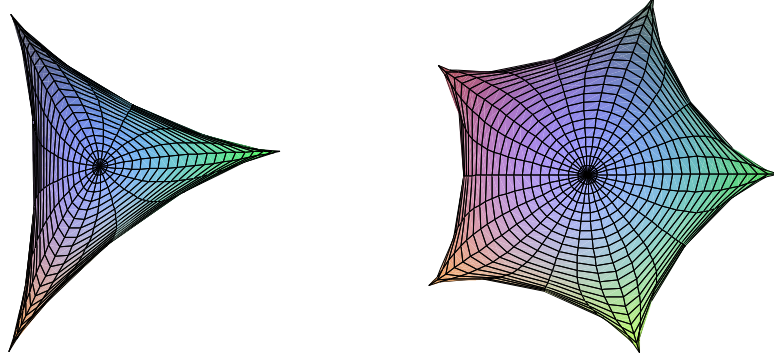


FIGURE 1. The image surface of the unit disc: (Left) $k = 3$, (Right) $k = 5$

- (3) and a singular point $x \in X$ is a swallowtail if and only if $q'(x) \neq 0$, $(q^3 \bar{q}' - q')(x) \neq 0$, and $\text{Re}(q''/q^2 - (3/2)(q')^2/q^3)(x) \neq 0$.

2.2. Solutions of the equation (A). The criterion in Lemma 2.1 applied to the case $q(x) = x^{k-2}$ shows that the hyperbolic Schwarz map in this case is singular along the unit circle $|x| = 1$, and has swallowtail singularities at the k -th roots of unity:

$$x = 1, \omega, \omega^2, \dots, \omega^{k-1}; \quad \omega = \exp(2\pi i/k).$$

The equation (A) is invariant under the change $x \mapsto \omega x$, and admits the solutions

$$(2.1) \quad u_0 = \sum_{n=0}^{\infty} a_n x^{kn} \quad \text{and} \quad u_1 = x \sum_{n=0}^{\infty} b_n x^{kn},$$

where

$$a_0 = 1, \quad a_n = \frac{a_{n-1}}{kn(kn-1)}; \quad b_0 = 1, \quad b_n = \frac{b_{n-1}}{kn(kn+1)}.$$

Relative to this choice of solutions, the k -fold symmetry of the equation yields the symmetry of S as the rotation by angle $2\pi/k$ around the y_3 -axis. Moreover, since the coefficients a_i and b_i are real, S is invariant under the reflection $(y_1, y_2, y_3) \mapsto (y_1, -y_2, y_3)$, which corresponds to $x \mapsto \bar{x}$.

The image of the unit disc is a k -gon with k -cuspidal vertices. Figure 1 shows the images of the unit disc when $k = 3$ and $k = 5$. Since the images for $k = 4, 5, \dots$ can be easily imagined from that for $k = 3$, we mainly work on this case.

2.3. Invariance of the hyperbolic Schwarz map. In the definition of the hyperbolic Schwarz map, we have freedom of choice of a pair of solutions. However, the map differs only by an isometric transformation of the ball \mathbf{B}^3 . For later use, we cite the following lemma:

Lemma 2.2. *Let $\{u_0, u_1\}$ and $\{v_0, v_1\}$ be two sets of independent solutions of the equation (E) that are related as $u_0 = c_1 v_0 + c_2 v_1$ and $u_1 = c_3 v_0 + c_4 v_1$. Let (y_1, y_2, y_3) (resp. (Y_1, Y_2, Y_3)) denote the coordinates of the image of the point x under the hyperbolic Schwarz map defined by use of $\{u_0, u_1\}$ (resp. $\{v_0, v_1\}$). Then*

both coordinates are related as follows.

$$\begin{aligned} y_1 &= \frac{A^0(1 + |Y|^2) + 2A^1Y_1 + 2A^2Y_2 + 2A^3Y_3}{2c(1 - |Y|^2) + D^0(1 + |Y|^2) + 2D^1Y_1 + 2D^2Y_2 + 2D^3Y_3}, \\ y_2 &= \frac{B^0(1 + |Y|^2) + 2B^1Y_1 + 2B^2Y_2 + 2B^3Y_3}{2c(1 - |Y|^2) + D^0(1 + |Y|^2) + 2D^1Y_1 + 2D^2Y_2 + 2D^3Y_3}, \\ y_3 &= \frac{C^0(1 + |Y|^2) + 2C^1Y_1 + 2C^2Y_2 + 2C^3Y_3}{2c(1 - |Y|^2) + D^0(1 + |Y|^2) + 2D^1Y_1 + 2D^2Y_2 + 2D^3Y_3}, \end{aligned}$$

where $c = |c_1c_4 - c_2c_3|$ and $|Y|^2 = Y_1^2 + Y_2^2 + Y_3^2$. The coefficients are determined as follows:

$$\begin{aligned} A^0 &= c_1\bar{c}_3 + \bar{c}_1c_3 + c_2\bar{c}_4 + \bar{c}_2c_4, & A^1 &= c_1\bar{c}_4 + \bar{c}_1c_4 + c_2\bar{c}_3 + \bar{c}_2c_3, \\ A^2 &= i(-c_1\bar{c}_4 + \bar{c}_1c_4 + c_2\bar{c}_3 - \bar{c}_2c_3), & A^3 &= c_1\bar{c}_3 + \bar{c}_1c_3 - c_2\bar{c}_4 - \bar{c}_2c_4, \\ B^0 &= i(c_1\bar{c}_3 - \bar{c}_1c_3 + c_2\bar{c}_4 - \bar{c}_2c_4), & B^1 &= i(c_1\bar{c}_4 - \bar{c}_1c_4 + c_2\bar{c}_3 - \bar{c}_2c_3), \\ B^2 &= c_1\bar{c}_4 + \bar{c}_1c_4 - c_2\bar{c}_3 - \bar{c}_2c_3, & B^3 &= i(c_1\bar{c}_3 - \bar{c}_1c_3 - c_2\bar{c}_4 + \bar{c}_2c_4), \\ C^0 &= c_1\bar{c}_1 + \bar{c}_2c_2 - c_3\bar{c}_3 - \bar{c}_4c_4, & C^1 &= c_1\bar{c}_2 + \bar{c}_1c_2 - c_3\bar{c}_4 - \bar{c}_3c_4, \\ C^2 &= i(-c_1\bar{c}_2 + \bar{c}_1c_2 + c_3\bar{c}_4 - \bar{c}_3c_4), & C^3 &= c_1\bar{c}_1 - \bar{c}_2c_2 - c_3\bar{c}_3 + \bar{c}_4c_4, \\ D^0 &= c_1\bar{c}_1 + \bar{c}_2c_2 + c_3\bar{c}_3 + \bar{c}_4c_4, & D^1 &= c_1\bar{c}_2 + \bar{c}_1c_2 + c_3\bar{c}_4 + \bar{c}_3c_4, \\ D^2 &= i(-c_1\bar{c}_2 + \bar{c}_1c_2 - c_3\bar{c}_4 + \bar{c}_3c_4), & D^3 &= c_1\bar{c}_1 - \bar{c}_2c_2 + c_3\bar{c}_3 - \bar{c}_4c_4. \end{aligned}$$

Proof is given by the identification of the hyperbolic space \mathbf{H}^3 and the 3-ball stated in Introduction.

Example 2.3. In the case where $c_1 = 1$, $c_2 = c_3 = 0$, and $|c_4| = 1$, we can see that

$$y_1 + iy_2 = c_4(Y_1 + iY_2) \quad \text{and} \quad y_3 = Y_3;$$

namely, the multiplication of u_1 by c_4 with u_0 unaltered corresponds to the rotation in the (y_1, y_2) -plane.

3. THE AIRY FUNCTIONS AND THE CONFLUENT HYPERGEOMETRIC FUNCTIONS

3.1. Properties of the Airy functions. The standard solutions of the equation (A) when $k = 3$ are the Airy function $Ai(x)$ defined by the Airy integral

$$Ai(x) = \frac{1}{\pi} \int_0^\infty \cos(t^3/3 + xt) dt$$

and the Airy function $Bi(x)$ of the second kind defined by the integral

$$Bi(x) = \frac{1}{\pi} \int_0^\infty (\exp(-t^3/3 + xt) + \sin(t^3/3 + xt)) dt.$$

We refer to [O, AS] for precise definitions of these integrals and the fundamental properties of these functions.

The solutions u_0 and u_1 in (2.1) are related with the Airy functions as follows:

$$(3.1) \quad u_0 = c_1 Ai(x) + c_2 Bi(x), \quad u_1 = c_3 Ai(x) + c_4 Bi(x),$$

where

$$\begin{aligned} c_1 &= 3^{2/3}\Gamma(2/3)/2, & c_2 &= 3^{1/6}\Gamma(2/3)/2, \\ c_3 &= -3^{5/6}\pi/(3\Gamma(2/3)), & c_4 &= 3^{1/3}\pi/(3\Gamma(2/3)). \end{aligned}$$

We denote by \mathcal{S}_A the hyperbolic Schwartz map relative to the set of solutions $\{u_0, u_1\}$ and by \mathcal{S}_T the map relative to the set $\{Ai, Bi\}$. It turns out that the former is better for drawing the surface because the symmetry is easily observed in the target and the latter is better for analyzing the behavior at infinity.

3.2. Asymptotic behavior of the Airy functions. In order to know the behavior as $|x|$ tends to infinity, we need to know the asymptotic behavior of the functions Ai and Bi . Since the differential equation is irregular singular, we need to take care of the Stokes lines. The Stokes line for the general equation (E) is by definition the curve satisfying

$$\operatorname{Re} \int_a^x \sqrt{q(t)} dt = 0,$$

where a is a root of $q = 0$; we refer to [F]. In the present case, they consist of three half-lines emanating from the origin:

$$x = r \exp(2\pi i/6), \quad x = -r, \quad x = r \exp(-2\pi i/6); \quad r \in [0, \infty).$$

The open cone bounded by two of these three lines is called a sector; we have three sectors:

$$\begin{aligned} S_0 &= \{r \exp(i\theta) \mid r > 0, -\pi/3 < \theta < \pi/3\}, \\ S_1 &= \{r \exp(i\theta) \mid r > 0, \pi/3 < \theta < \pi\}, \\ S_2 &= \{r \exp(i\theta) \mid r > 0, \pi < \theta < 5\pi/3\}. \end{aligned}$$

We cite the following lemma from [O], Chapter 11, Sections 1 and 8, pp.392–414.

Lemma 3.1. *When x lies inside the sector S_0 , the functions Ai and Bi have the following asymptotic expansions:*

$$\begin{aligned} Ai(x) &\sim \frac{e^{-\xi}}{2\sqrt{\pi}x^{1/4}} \sum_{s=0}^{\infty} (-1)^s \frac{a_s}{\xi^s}, & Ai'(x) &\sim -\frac{x^{1/4}e^{-\xi}}{2\sqrt{\pi}} \sum_{s=0}^{\infty} (-1)^s \frac{b_s}{\xi^s}, \\ Bi(x) &\sim \frac{e^{\xi}}{2\sqrt{\pi}x^{1/4}} \sum_{s=0}^{\infty} (-1)^s \frac{a_s}{\xi^s}, & Bi'(x) &\sim \frac{x^{1/4}e^{\xi}}{2\sqrt{\pi}} \sum_{s=0}^{\infty} (-1)^s \frac{b_s}{\xi^s}, \end{aligned}$$

where $x^{1/4}$ and $\xi = 2/3x^{3/2}$ take the principal values, and the coefficients a_s and b_s are defined as

$$a_0 = b_0 = 1, \quad a_s = \frac{(2s+1)(2s+3)\cdots(6s-1)}{(216)^s s!}, \quad b_s = -\frac{6s+1}{6s-1} a_s.$$

When x is real positive, they have the following expansions:

$$\begin{aligned} Ai(-x) &\sim \frac{1}{\sqrt{\pi}x^{1/4}} \left(\cos(\xi - \pi/4) \sum_{s=0}^{\infty} (-1)^s \frac{a_{2s}}{\xi^{2s}} + \sin(\xi - \pi/4) \sum_{s=0}^{\infty} (-1)^s \frac{a_{2s+1}}{\xi^{2s+1}} \right), \\ Ai'(-x) &\sim \frac{x^{1/4}}{\sqrt{\pi}} \left(\sin(\xi - \pi/4) \sum_{s=0}^{\infty} (-1)^s \frac{b_{2s}}{\xi^{2s}} - \cos(\xi - \pi/4) \sum_{s=0}^{\infty} (-1)^s \frac{b_{2s+1}}{\xi^{2s+1}} \right), \\ Bi(-x) &\sim \frac{1}{\sqrt{\pi}x^{1/4}} \left(-\sin(\xi - \pi/4) \sum_{s=0}^{\infty} (-1)^s \frac{a_{2s}}{\xi^{2s}} + \cos(\xi - \pi/4) \sum_{s=0}^{\infty} (-1)^s \frac{a_{2s+1}}{\xi^{2s+1}} \right), \\ Bi'(-x) &\sim \frac{x^{1/4}}{\sqrt{\pi}} \left(\cos(\xi - \pi/4) \sum_{s=0}^{\infty} (-1)^s \frac{b_{2s}}{\xi^{2s}} + \sin(\xi - \pi/4) \sum_{s=0}^{\infty} (-1)^s \frac{b_{2s+1}}{\xi^{2s+1}} \right). \end{aligned}$$

3.3. The confluent hypergeometric functions. The *confluent hypergeometric differential equation* is defined as

$$(3.2) \quad xu'' + (\gamma - x)u' - \alpha u = 0,$$

where α and γ are constants. We assume here that these constants are real. It is regular singular at $x = 0$ and irregular singular at $x = \infty$. By a change of the unknown u by multiplying a non-zero function

$$\rho = e^{-x/2}x^{\gamma/2},$$

and a change of parameters

$$(3.3) \quad a = 2\alpha - \gamma, \quad b = \gamma^2 - 2\gamma,$$

this equation transforms to the equation (C). We have an apparent symmetry $(x, a, b) \leftrightarrow (-x, -a, b)$ and note that the Bessel differential equation corresponds to the case $a = 0$. As we showed in [SSY], The associated hyperbolic Schwarz map behaves differently according as $a = 0$ or $a \neq 0$. An ordinary set of independent solutions of (3.2) is given as

$$f_1(x) = F(\alpha, \gamma; x) \quad \text{and} \quad f_2(x) = x^{1-\gamma}F(\alpha - \gamma + 1, 2 - \gamma; x),$$

unless γ is not integer, where

$$F(\alpha, \gamma; x) = \sum_{k=0}^{\infty} \frac{(\alpha, k)}{(\gamma, k)k!} x^k$$

is the confluent hypergeometric function and $(c, k) = c(c+1)\cdots(c+k-1)$. Hence,

$$u_0 = \rho(x)f_1(x) \quad \text{and} \quad u_1 = \rho(x)f_2(x)$$

make a set of independent solutions of (C). Since we need the asymptotic behaviors of solutions, we cite the following lemma from [O], p.256:

Lemma 3.2. *There exist two solutions U and V that have the following asymptotic expansions.*

$$U(\alpha, \gamma; x) \sim x^{-\alpha} \sum_{k=0}^{\infty} (-1)^k \frac{(\alpha, k)(1 + \alpha - \gamma, k)}{k!x^k}, \quad |\arg x| \leq 3\pi/2 - \delta,$$

$$V(\alpha, \gamma; x) \sim e^x (-x)^{\alpha-\gamma} \sum_{k=0}^{\infty} \frac{(\gamma - \alpha, k)(1 - \alpha, k)}{k!x^k}, \quad |\arg(-x)| \leq 3\pi/2 - \delta,$$

for any positive small number δ . They are well-defined even if γ is an integer.

The relations of these solutions with the functions f_1 and f_2 are given as

$$U = \frac{\pi}{\sin \pi \gamma} \left(\frac{f_1}{\Gamma(\alpha - \gamma + 1)\Gamma(\gamma)} - \frac{f_2}{\Gamma(\alpha)\Gamma(2 - \gamma)} \right),$$

$$V = \frac{\pi}{\sin \pi \gamma} \left(\frac{f_1}{\Gamma(1 - \alpha)\Gamma(\gamma)} - \frac{e^{\pi i}(\gamma - 1)f_2}{\Gamma(\gamma - \alpha)\Gamma(2 - \gamma)} \right),$$

with the convention $\arg(-x) = \arg(x) - \pi$; we refer to [AS], Chapter 13, pp.504–505.

We next set

$$(3.4) \quad v_0 = \rho(x)U(x) \quad \text{and} \quad v_1 = \rho(x)V(x)$$

and denote by \mathcal{S}_C the hyperbolic Schwarz map relative to this set. From Lemma 3.2, we have the following.

Lemma 3.3. *The solutions v_0 and v_1 have the asymptotic expansions as*

$$(3.5) \quad v_0 = \rho U(x) \sim e^{-x/2}x^{-a} \left(1 - \frac{\alpha(a + \alpha - \gamma)}{x} + O\left(\frac{1}{x^2}\right) \right),$$

$$v_1 = \rho V(x) \sim e^{x/2}(-x)^a \left(1 + \frac{(\gamma - \alpha)(1 - \alpha)}{x} + O\left(\frac{1}{x^2}\right) \right)$$

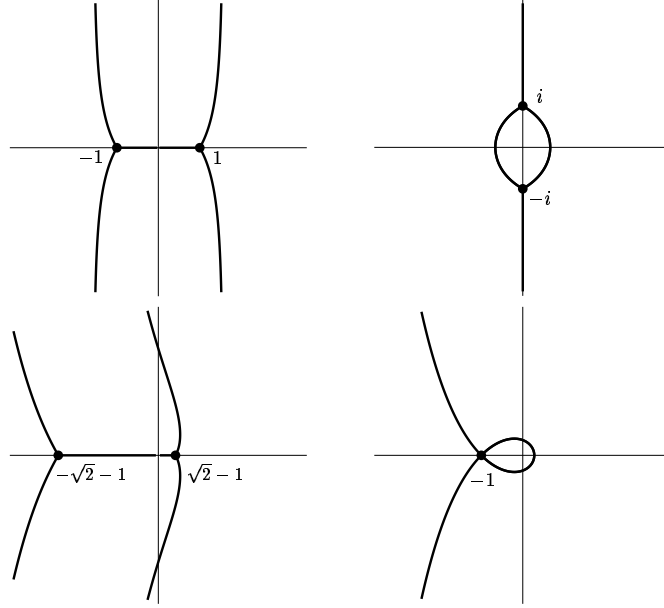


FIGURE 2. Stokes lines for the confluent hypergeometric equation

that are valid in the common domain $-\pi/2 + \delta \leq \arg(x) \leq 3\pi/2 - \delta$ for any positive small number δ .

3.4. Stokes lines of the confluent hypergeometric functions. We exhibit the Stokes lines in some cases in Figure 2; The authors are grateful to Tatsuya Koike who provided these figures. The figures are arranged from left to right and from upper to lower with the parameters as $a = 0, b = -1$; $a = 0, b = 1$; $a = 1, b = -1$ and $a = 1, b = 1$; the small dots in the figures denote the points $q = 0$.

Although the shapes of the figures change fairly drastically, the asymptotic behavior of solutions at infinity turns out to be simple as we will see in Section 5. This is because the the Stokes lines approach to the infinity from two directions irrespective of the parameters. Indeed, the differential equation relative to the variable $t = 1/x$ is written as

$$\ddot{v} - \frac{1 + 2at + bt^2}{4t^4}v = 0,$$

which means $\sqrt{q} \sim 1/(2t^2)$ at $t = 0$ and, if we set $t = \epsilon e^{i\theta}$ for small ϵ , then $\int \sqrt{q} dt \sim -(1/2\epsilon)e^{-i\theta}$; hence, the Stokes lines approach the infinity along the direction $\theta = \pm\pi/2$, namely along the imaginary axis.

4. IMAGE SURFACE FOR THE AIRY DIFFERENTIAL EQUATION

4.1. Image of a fan around the line $\arg x = 0$. In Figure 3, we draw the Stokes lines and the sectors. The round circle denotes $|x| = 1$. The image of the fan

$$\{x \in X \mid |\arg x| < \frac{\pi}{6}, 0.7 < |x| < 1.5\}$$

is shown in Figure 4, where a swallowtail singularity can be seen. Since around any swallowtail singularity the surface must self-intersect, we can trace the self-intersection curve: its preimage in the sector S_0 and its equivalents in the other sectors are drawn in Figure 3. Each curve is a simple curve touching the unit circle at $x = 1$, and approaching asymptotically to the real axis or to its equivalents.

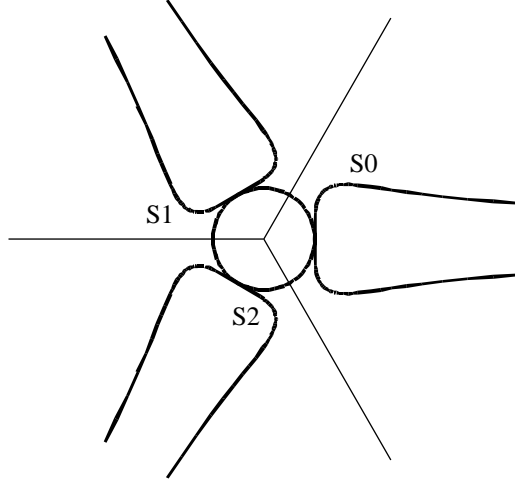
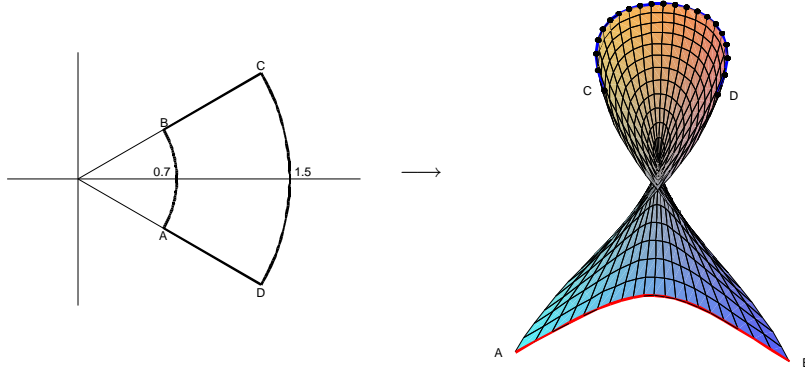


FIGURE 3. Stokes lines and sectors

FIGURE 4. Image of a fan around the line $\arg x = 0$

Here and in the following, we use Maple 9.5 for a practical computation of functions A_i and B_i .

4.2. Image of a fan around the line $\arg x = \pi/3$. The image of the fan

$$\{x \in X \mid \left| \arg x - \frac{\pi}{3} \right| < a\}$$

looks like a winding paper. Figure 5 is the image of such a fan with $0.5 < |x| < 4.5$ and $a = \pi/64$; the cuspidal edge curve (image of $|x| = 1$) can be seen inside the roll.

4.3. Image of rings around the origin. The functions $A_i(x)$ and $B_i(x)$ have infinite number of zeros on the negative real axis. Let $[-r_1, -r_2, -r_3, \dots]$ be the zeros of A_i and $[-s_1, -s_2, -s_3, \dots]$ the zeros of B_i , both in decreasing order. They are interlacing each other: $s_i < r_i < s_{i+1}$. For example, $s_1 = 1.1737$ and $r_1 = 2.3381$. Here, we show the images of the thin four rings $s_1 \leq |x| \leq 1.5$, $1.5 \leq |x| \leq 1.8$, $1.8 \leq |x| \leq 2.1$ and $2.1 \leq |x| \leq r_1$ in Figure 6, which are viewed from the same angle. They change their shapes gradually but they look having the same homotopy. The union of the four figures is redrawn in Figure 8.

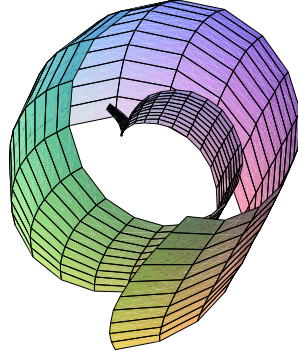
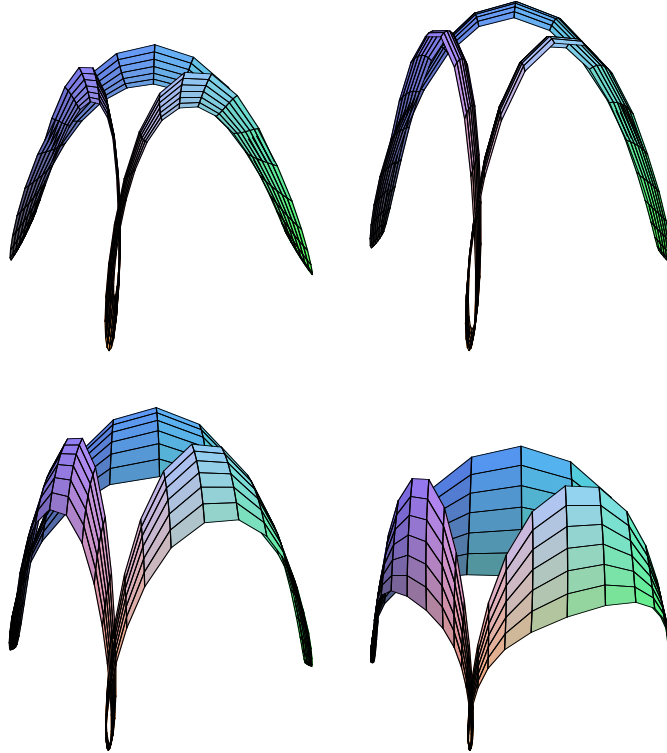
FIGURE 5. Image of a fan around the line $\arg x = \pi/3$ 

FIGURE 6. Images of rings

The hyperbolic Schwarz map \mathcal{S}_T associated with the set $\{Ai, Bi\}$ is written as

$$\mathbf{C} \ni x \mapsto \frac{1}{L}(P, Q, R) \in \mathbf{B}^3,$$

where

$$L = 2/\pi + |Ai|^2 + |Ai'|^2 + |Bi|^2 + |Bi'|^2, \quad P = 2\text{Re}(Ai\overline{Bi}) + 2\text{Re}(Ai'\overline{Bi}'),$$

$$Q = 2\text{Im}(Ai\overline{Bi}) + 2\text{Im}(Ai'\overline{Bi}'), \quad R = |Ai|^2 + |Ai'|^2 - |Bi|^2 - |Bi'|^2,$$

where $AiBi' - BiAi' = 1/\pi^2$ is used. Relying on these expressions, we have the following.

Proposition 4.1. *The image $\mathcal{S}_T(x)$ of the hyperbolic Schwarz map tends to $(0, 0, -1)$ as $|x|$ tends to infinity while it remains in the sector S_0 . The image $\mathcal{S}_T(-x)$ of the negative real axis has no limit when x tends to infinity; however the set of accumulation of such points is the whole circle on the boundary sphere that is the section by the plane $y_2 = 0$.*

Proof. Assume $|\arg x| \leq \pi/3$. Then it is straightforward to see that

$$\begin{aligned} L(x) &\sim \frac{(x\bar{x})^{1/4} e^{\xi+\bar{\xi}}}{\pi} \left(1 + O\left(\frac{1}{\xi}\right)\right), \\ P(x) &\sim \operatorname{Re} \frac{e^{-\xi+\bar{\xi}}}{\pi(x\bar{x})^{1/4}} \left(1 + \frac{a_1}{\xi} - \frac{a_1}{\xi} + O\left(\frac{1}{\xi^2}\right)\right) - \operatorname{Re} \frac{(x\bar{x})^{1/4} e^{-\xi+\bar{\xi}}}{\pi} \left(1 + \frac{b_1}{\xi} - \frac{b_1}{\xi} + O\left(\frac{1}{\xi^2}\right)\right), \\ Q(x) &\sim \operatorname{Im} \frac{e^{-\xi+\bar{\xi}}}{\pi(x\bar{x})^{1/4}} \left(1 + \frac{a_1}{\xi} - \frac{a_1}{\xi} + O\left(\frac{1}{\xi^2}\right)\right) - \operatorname{Im} \frac{(x\bar{x})^{1/4} e^{-\xi+\bar{\xi}}}{\pi} \left(1 + \frac{b_1}{\xi} - \frac{b_1}{\xi} + O\left(\frac{1}{\xi^2}\right)\right), \\ R(x) &\sim \frac{e^{-\xi-\bar{\xi}}}{4\pi(x\bar{x})^{1/4}} \left(1 - \frac{a_1}{\xi} - \frac{a_1}{\xi} + O\left(\frac{1}{\xi^2}\right)\right) - \frac{e^{\xi+\bar{\xi}}}{\pi(x\bar{x})^{1/4}} \left(1 + \frac{a_1}{\xi} + \frac{a_1}{\xi} + O\left(\frac{1}{\xi^2}\right)\right) \\ &\quad + \frac{(x\bar{x})^{1/4} e^{-\xi-\bar{\xi}}}{4\pi} \left(1 - \frac{b_1}{\xi} - \frac{b_1}{\xi} + O\left(\frac{1}{\xi^2}\right)\right) - \frac{(x\bar{x})^{1/4} e^{\xi+\bar{\xi}}}{\pi} \left(1 + \frac{b_1}{\xi} + \frac{b_1}{\xi} + O\left(\frac{1}{\xi^2}\right)\right). \end{aligned}$$

We set $x = r \exp(i\theta)$ and assume $|\theta| \leq \pi/3 - \delta$ for some positive constant δ . Then $\xi + \bar{\xi} = 2/3r^{3/2} \cos(3\theta/2)$ and $1/\xi - 1/\bar{\xi} = 3ir^{-3/2} \sin(3\theta/2)$ show that $P/L \sim 0$, $Q/L \sim 0$ and $R/L \sim -1$, uniformly for each δ . Hence we have the first statement. For the second statement we use

$$\begin{aligned} L(-x) &\sim \frac{2}{\pi} + \frac{\sqrt{x}}{\pi} \left(1 + O\left(\frac{1}{\xi^2}\right)\right) + \frac{1}{\pi\sqrt{x}} \left(1 + O\left(\frac{1}{\xi}\right)\right), \\ P(-x) &\sim \left(\frac{1}{\pi\sqrt{x}} - \frac{\sqrt{x}}{\pi}\right) \left(\cos(2\xi) + O\left(\frac{1}{\xi}\right)\right), \\ Q(-x) &= 0, \\ R(-x) &\sim \left(\frac{1}{\pi\sqrt{x}} - \frac{\sqrt{x}}{\pi}\right) \left(\sin(2\xi) + O\left(\frac{1}{\xi}\right)\right), \end{aligned}$$

for real positive x . Hence we have the result. \square

We remark that the image $\mathcal{S}_T(x)$ of $x \in S_1$ tends to $(0, -1, 0)$ and that of $x \in S_2$ to $(0, 1, 0)$. This result is transferred to the map \mathcal{S}_A associated with the set $\{u_0, u_1\}$:

Corollary 4.2. *The image \mathcal{S}_A tends to the following respective points as $|x|$ tends to infinity while it remains in the sectors S_0 , S_1 and S_2 :*

$$\begin{aligned} p_0 &= (k_1, 0, k_3), \\ p_1 &= (k_1 \cos(2\pi/3), k_1 \sin(2\pi/3), k_3), \\ p_2 &= (k_1 \cos(4\pi/3), k_1 \sin(4\pi/3), k_3), \end{aligned}$$

where

$$\begin{aligned} k_1 &= \frac{4\pi 3^{5/6} \Gamma(2/3)^2}{3^{5/3} \Gamma(2/3)^4 + 4\pi^2} \sim 0.95204 \ 89606, \\ k_3 &= \frac{3^{5/3} \Gamma(2/3)^4 - 4\pi^2}{3^{5/3} \Gamma(2/3)^4 + 4\pi^2} \sim -0.30594 \ 57086. \end{aligned}$$

The images \mathcal{S}_A of the three Stokes lines $\{|x| \arg(x) = \pi/3\}$, $\{|x| \arg(x) = \pi\}$ and $\{|x| \arg(x) = -\pi/3\}$ tend to the boundary circles, which are the sections of the

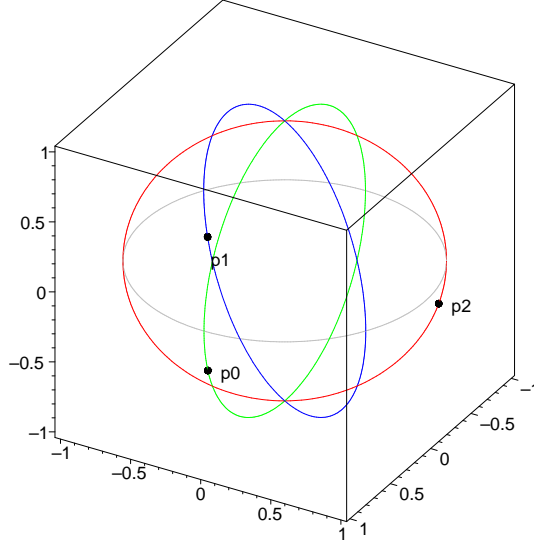


FIGURE 7. Limits of $|x| = \infty$

boundary ball by the planes that are equidistant from p_0 and p_1 , p_1 and p_2 , and p_2 and p_0 , respectively. They meet at the poles $(0, 0, \pm 1)$.

Proof. Since $(k_1, 0, k_3)$ is the transform of $(Y_1, Y_2, Y_3) = (0, 0, -1)$, Lemma 2.2 shows that

$$k_1 = \frac{2c_2c_4}{c_2^2 + c_4^2} \quad \text{and} \quad k_3 = \frac{c_2^2 - c_4^2}{c_2^2 + c_4^2}.$$

□

These figures are shown in Figure 7. Note that p_2 lies on the first circle, and p_0 on the second and p_1 on the third.

4.4. Change of image of rings. The map \mathcal{S} on the negative real axis is approximately equal to $(-\cos(2\xi), 0, -\sin(2\xi))$ where $\xi = (2/3)|x|^{3/2}$, which is periodic relative to ξ . We here note that the zeros of $\cos(2\xi)$ for negative x are $-(3\pi(2m-1)/8)^{2/3}$, and that these values are the asymptotic values of zeros of either $Ai(x)$ or $Bi(x)$; refer to 10.4.94 and 10.4.98 in [AS], Chapter 10. Hence, it is natural to look at the images of rings

$$S_i = \mathcal{S}_A(\{x \mid s_i \leq |x| \leq r_i\}) \quad \text{and} \quad R_i = \mathcal{S}_A(\{x \mid r_i \leq |x| \leq s_{i+1}\}),$$

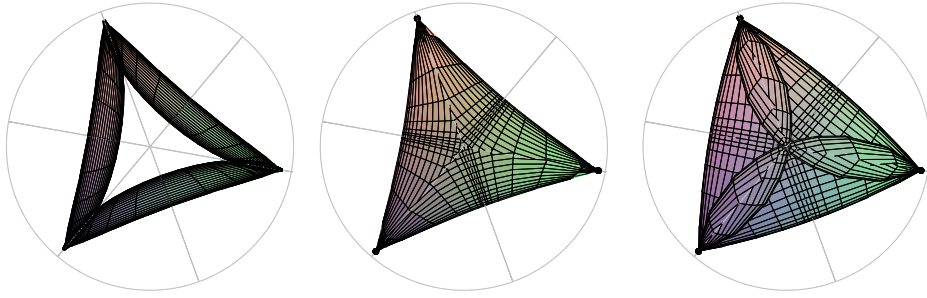
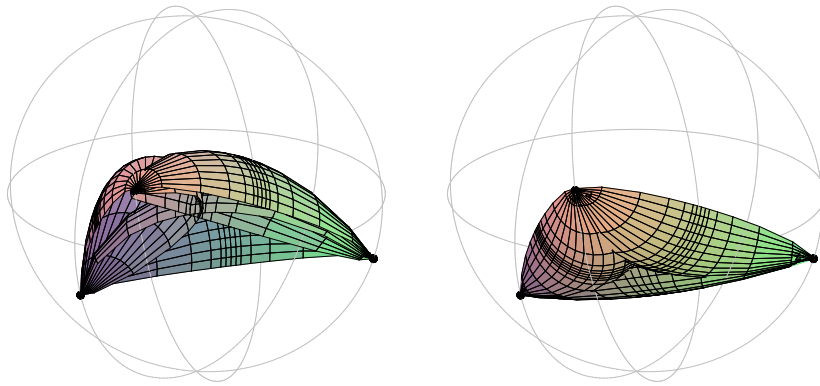
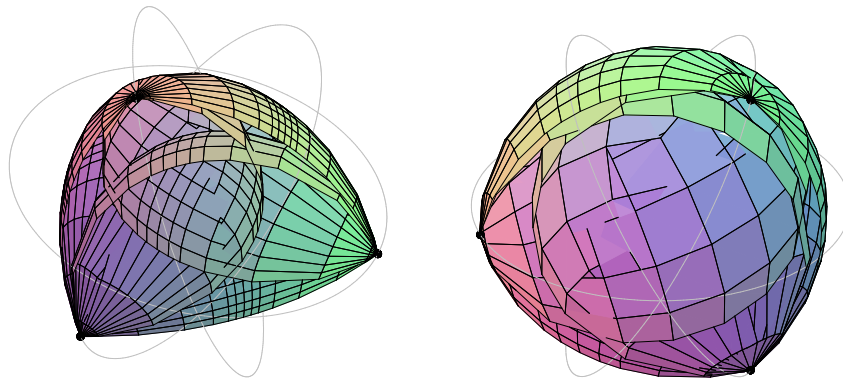
where s_i and r_i denote the zeros defined in Subsection (4.3). We found the following experimental fact.

In Figure 8 we draw the images of three rings S_1 , R_1 and S_2 viewed in the same angle; note that the image of S_1 is the union of four figures in Figure 6.

Figure 9 gives the view of the images of S_2 and R_2 from the different point of view; they can be glued continuously. We note that R_2 looks just like the mirror of S_2 .

The left figure of Figure 10 is S_{10} and the right is S_{100} .

Note that $s_2 = 3.2710$, $r_2 = 4.0879$, $s_3 = 4.8307$, $s_{10} = 12.3864$, $r_{10} = 12.8287$, $s_{11} = 13.2636$, $s_{100} = 60.2533$, $r_{100} = 60.4555$, $s_{101} = 60.6574$.

FIGURE 8. Images of the rings S_1 , R_1 and S_2 FIGURE 9. Images of the rings S_2 and R_2 FIGURE 10. Images of the rings S_{10} and S_{100}

To see more finely the right figure of Figure 10, we draw in Figure 11 the images of the circles lying in S_{100} in the left column and the circles lying in R_{100} in the right column. The left of each pair draws the curve viewed in the direction of angle $[25, 100]$ (i.e., the viewer's point is near the north pole) and the right in the direction of angle $[80, 85]$ (the viewer's point is near the horizontal plane). The dotted points are p_0 , p_1 and p_2 and the grey circles denote those given in Figure 7.

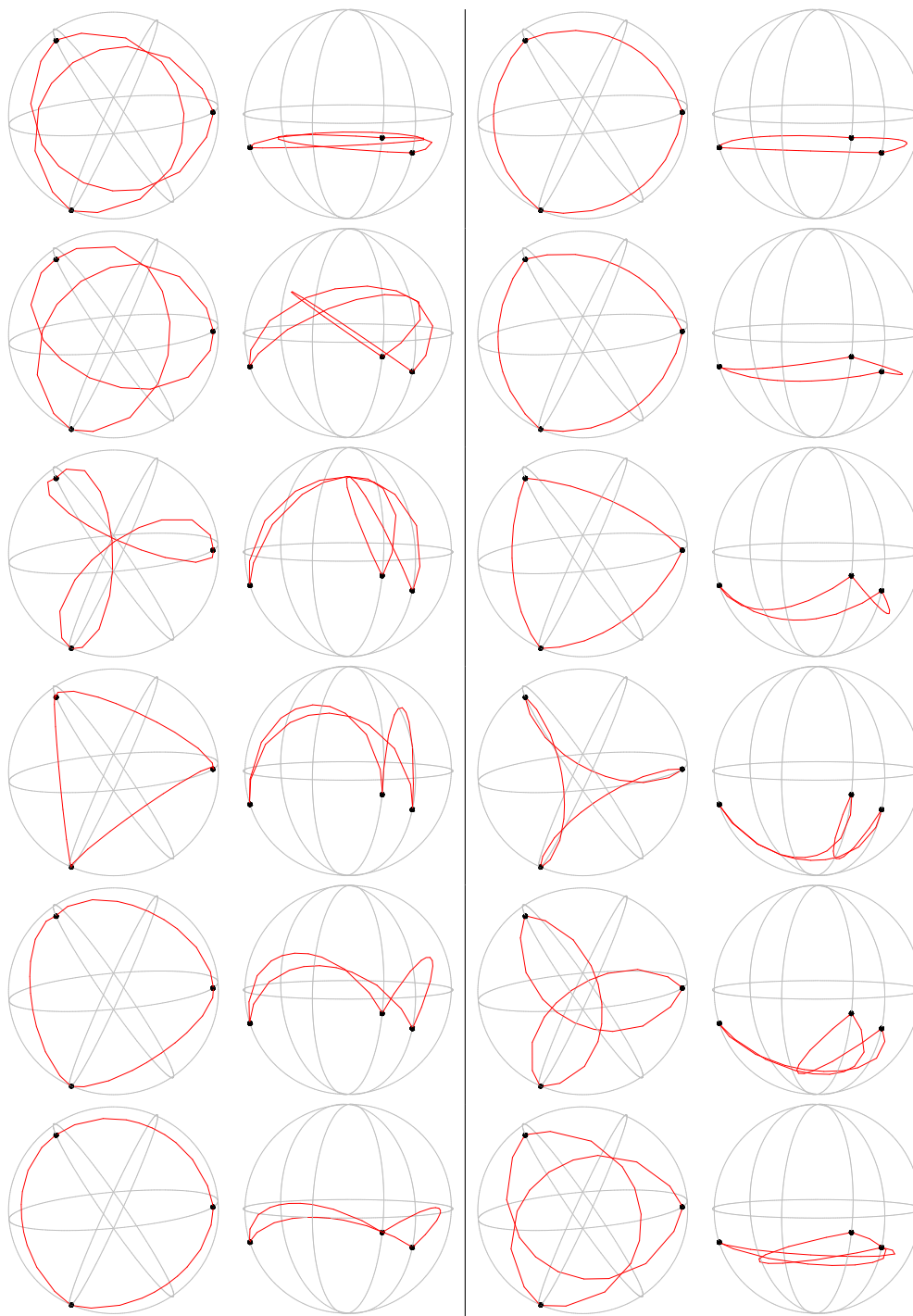


FIGURE 11. Images of circles in the rings $s_{100} \leq |x| \leq r_{100}$ (left) and $r_{100} \leq |x| \leq s_{101}$ (right)

5. ASYMPTOTIC BEHAVIOR OF THE HYPERBOLIC SCHWARZ MAP ASSOCIATED WITH THE CONFLUENT HYPERGEOMETRIC EQUATION

The asymptotic behavior the hyperbolic Schwarz map associated with the confluent hypergeometric equation can be examined analogously as in the proof of Proposition 4.1. We use the same notations L , P , Q and R in Section 4.3 applied to the set $\{v_0, v_1\}$ in (3.4). Then we have

$$\begin{aligned} L &\sim 2 + \frac{5}{4} \left| x^{-a/2} e^{-x/2} \right| + \frac{5}{4} \left| (-x)^{a/2} e^{x/2} \right|, \\ P &\sim \frac{3}{4} (-x/\bar{x})^{-a/2} e^{(\bar{x}-x)/2} + \frac{3}{4} (-\bar{x}/x)^{-a/2} e^{(x-\bar{x})/2}, \\ Q &\sim -i \frac{3}{4} (-x/\bar{x})^{-a/2} e^{(\bar{x}-x)/2} + i \frac{3}{4} (-\bar{x}/x)^{-a/2} e^{(x-\bar{x})/2}, \\ R &\sim \frac{5}{4} \left| x^{-a/2} e^{-x/2} \right| - \frac{5}{4} \left| (-x)^{a/2} e^{x/2} \right|, \end{aligned}$$

when $|x|$ is large, up to higher order terms of $1/x$. We set $z = r \exp(i\theta)$. Then, if $a = 0$, we see that

$$\begin{aligned} L &\sim 2 + \frac{5}{4} (\exp(-r \cos \theta) + \exp(r \cos \theta)), & R &\sim \frac{5}{4} (\exp(-r \cos \theta) - \exp(r \cos \theta)), \\ P &\sim \frac{3}{2} \cos(-r \sin \theta), & Q &\sim \frac{3}{2} \sin(-r \sin \theta), \end{aligned}$$

which show

$$\lim \frac{1}{L} (P, Q, R) = (0, 0, -1) \quad \text{or} \quad (0, 0, 1)$$

according as $\cos \theta > 0$ or $\cos \theta < 0$, while, when $\cos \theta = 0$, the point approaches to any point in the circle

$$(5.1) \quad C := \{(y_1, y_2, 0) \mid y_1^2 + y_2^2 = 1/9\}.$$

If $a \neq 0$, then P and Q remain bounded and

$$L \sim \frac{5}{4} r^a \exp(r \cos \theta) \quad \text{and} \quad R \sim -\frac{5}{4} r^a \exp(r \cos \theta)$$

when $\cos \theta > 0$, and

$$L \sim \frac{5}{4} r^{-a} \exp(-r \cos \theta) \quad \text{and} \quad R \sim \frac{5}{4} r^{-a} \exp(-r \cos \theta)$$

when $\cos \theta < 0$. Furthermore, when $\cos \theta = 0$, we see that

$$L \sim 2 + \frac{5}{4} (r^a + r^{-a}) \quad \text{and} \quad R \sim \frac{5}{4} (r^{-a} - r^a).$$

Thus we have the following statement.

Proposition 5.1. *We divide the x -plane into three parts: $N = \{x \mid \operatorname{Re}(x) < 0\}$, $L = \{x \mid \operatorname{Re}(x) = 0\}$ and $P = \{x \mid \operatorname{Re}(x) > 0\}$, and denote by NP , SP and C the north pole $(0, 0, 1)$, the south pole $(0, 0, -1)$ and the circle (5.1). Then the point $\mathcal{S}_C(x)$ tends to NP or SP , or accumulates to C as follows.*

	$a < 0$	$a = 0$	$a > 0$
N	NP	NP	NP
L	SP	C	NP
P	SP	SP	SP

To have an intuitive image, we draw some pictures: Figure 12 draws the image under \mathcal{S}_C relative to the set of solutions $\{v_0, v_1\}$ in (3.4) of three half-lines $\{x \mid \arg(x) = \pi/4\}$ (blue), $\{x \mid \arg(x) = \pi/2\}$ (red) and $\{x \mid \arg(x) = 3\pi/4\}$ (green). The parameters are taken as indicated in the figure. The grey-colored curves are the great circles for reference.

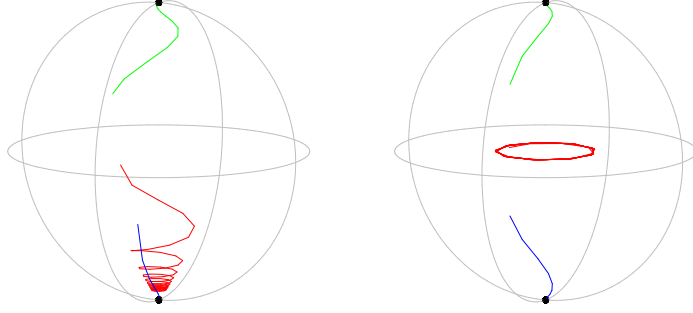


FIGURE 12. Parameters: $\alpha = 1/2$ and $\gamma = 1/4$ [$a > 0$] (left); $\alpha = 1/4$ and $\gamma = 1/2$ [$a = 0$] (right)

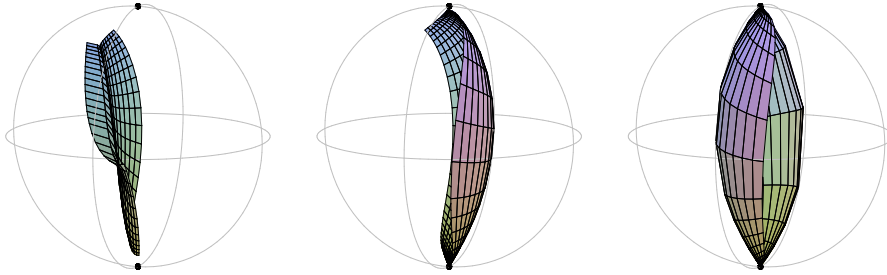


FIGURE 13. Image surfaces when $a = 1$, $b = -16/25$; $(r_1, r_2) = (0.2, 2), (2, 5), (5, 10)$.

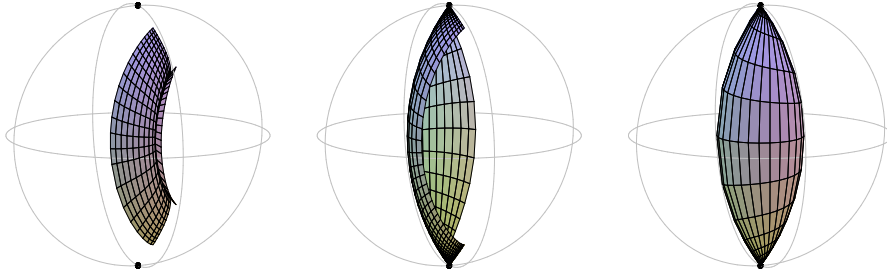


FIGURE 14. Image surfaces when $a = 0$, $b = -3/4$; $(r_1, r_2) = (0.2, 2), (2, 5), (5, 10)$.

The last figures Figures 13-14 show several images of the area $\{x = re^{i\theta} \mid r \in [r_1, r_2], \theta \in [0, \pi]\}$. In the first row, the values of parameters are $\alpha = 13/5$, $\gamma = 8/5$, i.e., $a = 1$, $b = -16/25$ and $r \in [0.2, 2], [2, 5]$ and $[5, 10]$. As we saw in [SSY], the first surface contains the cuspidal edge curve and two swallowtail singularities, which may not be seen; refer to [SSY] for finer pictures near the point $x = 0$. In the second row, the values are $\alpha = 1/4$, $\gamma = 1/2$, i.e., $a = 0$, $b = -3/4$ and $r \in [0.2, 2], [2, 5]$ and $[5, 10]$; in this case, the cuspidal edge is smooth and the surface has no swallowtails.

ACKNOWLEDGMENTS

While in preparation of the paper, the authors enjoyed the several discussions with H. Majima, W. Rossman and T. Koike, to whom they would like to express their thanks.

REFERENCES

- [AS] M. ABRAMOWITZ AND I. A. STEGUN, *Handbook of Mathematical Functions*, Dover Publ., New York, 1965.
- [F] M. V. FEDORYUK, *Asymptotic Analysis*, Springer Verlag, Berlin, 1993.
- [KRSUY] M. KOKUBU, W. ROSSMAN, K. SAJI, M. UMEHARA AND K. YAMADA, *Singularities of flat fronts in hyperbolic space*, Pacific J. Math. **221**(2005), 303–351.
- [NSYY] M. NORO, T. SASAKI, K. YAMADA AND M. YOSHIDA, *Confluence of swallowtail singularities of the hyperbolic Schwarz map defined by the hypergeometric differential equation*, preprint 2007.
- [O] F. W. J. OLVER, *Asymptotics and Special Functions*, AK̃Peters, Massachusettes, 1997. (Originally published by Academic Press, New York, 1974.)
- [SSY] K. SAJI, T. SASAKI, AND M. YOSHIDA, *Hyperbolic Schwarz map of the confluent hypergeometric differential equation*, preprint 2007.
- [SYY1] T. SASAKI K. YAMADA AND M. YOSHIDA, *Hyperbolic Schwarz map for the hypergeometric equation*, to appear in Experimental Math., (arXiv:math/0609196; revised 2007).
- [SYY2] T. SASAKI K. YAMADA AND M. YOSHIDA, *Derived Schwarz map of the hypergeometric differential equation and a parallel family of flat fronts*, to appear in Intern. J. Math., (arXiv:math/0702863).
- [Y] M. YOSHIDA, *Hypergeometric Functions, My Love*, Vieweg Verlag, Wiesbaden, 1997.

(Sasaki) DEPARTMENT OF MATHEMATICS, KOBE UNIVERSITY, KOBE 657-8501, JAPAN
E-mail address: sasaki@math.kobe-u.ac.jp

(Yoshida) FACULTY OF MATHEMATICS, KYUSHU UNIVERSITY, FUKUOKA 810-8560, JAPAN
E-mail address: myoshida@math.kyushu-u.ac.jp